Journal of Contemporary Technology and Applied Engineering (JCTAE)
Home Page: https://jctae.journals.ekb.eg/
Published by: Faculty of Engineering, Kafrelsheikh University

Volume: 3 Issue: 2 Year: 2025
Pages: 16 – 28
DOI: 10.21608/jctae.2024.329091.1036
Print ISSN: 2812-5797
Online ISSN: 2812-5800

COGENERATION PERFORMANCE ANALYSIS OF THERMAL AND ELECTRICAL EFFICIENCY IN VARIOUS GLAZED PHOTOVOLTAIC/THERMAL (PV/T) CONFIGURATIONS

Received: 17-10-2024
Accepted: 13-11-2024

Amr Elbrashy[a,b,*], Magda El-fakharany[a,b], Maher Abo Elsood[b], Fawzy Abou-Taleb[b], Fadl A. Essa[b,*]

[a] *Department of Mechatronics, Faculty of Engineering, Horus University-Egypt (HUE), New Damietta, 34517, Egypt*
[b] *Mechanical Engineering Department, Faculty of Engineering, Kafrelsheikh University, Kafrelsheikh 33516, Egypt,*
[*] Corresponding authors: A. Elbrashy (amr_pg097@eng.kfs.edu.eg); F. A. Essa (fadlessa@eneg.kfs.edu.eg)

ABSTRACT. Cogeneration power systems are a key area for improving energy efficiency by minimizing losses. This paper presents a theoretical investigation into the thermal and electrical performance of an enhanced photovoltaic/thermal (PV/T) system. A refined thermo-electrical model is developed to evaluate key performance parameters, including thermal and electrical aspects. The model incorporates advanced correlations for radiative heat losses and considers radiation heat transfer within the air duct. Four distinct system models are compared: (I) a glazing photovoltaic panel, (II) a glazing PV/T cogeneration system, (III) a glazing PV/T system with an absorber plate, and (IV) a glazing double-pass PV/T cogeneration system with an absorber layer. Analytical solutions are validated using experimental data from previous studies, with representative weather data from Egypt. Results show that model IV achieves the highest efficiency at 92% under peak solar radiation (12:00 PM), followed by Model III at 77%, while models I and II yield lower efficiencies of 29% and 61%, respectively.

KEYWORDS: PV/T; Hybrid system; Cogeneration; Thermal performance; Energy efficiency.

1. INTRODUCTION

Renewable and clean energy are now widely supported worldwide because conventional energy sources are limited, people are more aware of environmental problems, and many renewable energy sources exist. Solar has stood out among these green energy sources because it is easy for many people to access. Solar energy can be turned into electricity using photovoltaic cells. These cells make electricity when solar light interacts with semiconductor material [1, 2]. These days, photovoltaic solar panels are being used more and more in building facades, photovoltaic gardens, tiles, awnings, Venetian blinds, and other design elements. Every day when it's sunny, the earth receives more than 15,000 times the world's total energy use and 100 times the world's coal, gas, and oil supplies. [3, 4]. A device like a photovoltaic cell can convert 9-20% of the sun's rays into usable electricity, depending on the technology used to make the cell. This electricity can then be used to power homes, businesses, and even entire communities, reducing the reliance on fossil fuels and decreasing greenhouse gas emissions. As technology continues to improve, the efficiency of solar cells is expected to increase, making solar energy an even more viable and sustainable source of power for the future [5].

The photovoltaic panels in their commercial presentation absorb 20% of the incident solar radiation to generate electricity, and the remaining 80% is transformed into heat, elevating the temperature of the cells over 50°C. This increase in temperature causes a decrease in the efficiency of the cells by 0.4% per degree Celsius above 25 °C [6]. In order to reduce the temperature of the cells and improve their capacity to transform solar energy into electricity, PV/T (photovoltaic-thermal) cogeneration collectors were developed, a combination of a thermal collector and a photovoltaic panel. In photovoltaic thermal cogeneration collectors, the possible use of the heat generated by the PV panels can increase the efficiency of the panels, i.e., photovoltaic is capable of generating thermal energy and electrical energy simultaneously, which can be used in different applications such as air and water heating, dryers, desalination, and others, depending on the type of connection of the elements of the collector [7].

Limane, et al. [8] employed a transient 3D finite element method (FEM)-based model to simulate the PV panel's behavior. The study also includes a parametric analysis to investigate the effects of different factors on PV performance. The study also highlighted that in Adrar, Algeria, a PV panel inclined at 45° produced the highest electrical power despite elevated cell temperatures. Moreover, they recommended forced convection as the most effective cooling method for PV cells. They suggested a minimum distance of 150 mm between the ground and the PV panel to ensure adequate airflow and maximize electrical production.

Herrando, et al. [9] Created a comprehensive CFD model of an exposed water-based PV/T collector with a roll-bond aluminium thermal absorber. The main objectives were to examine the flow inside the absorber channels and the temperature distribution of the collector. A temperature differential of approximately 5 °C was noted between the channels next to the collector intake and those in the center. The non-uniform temperature distribution resulted in an approximate 8% decrease in photovoltaic cell performance between the collector's hottest and most remarkable areas. To address this issue, the research suggested altering the widths of specific channels to enhance their pressure drop, thereby attaining a more consistent fluid flow rate. The results indicated that thermal efficiency fluctuated between 51% and 3.4% for fluid input temperatures of 20 °C to 70 °C at the nominal flow rate. Still, electrical efficiency varied from 18.5% to 15.2% within the same temperature range.

Hamada, et al. [10] investigated the use of nano-encapsulated phase change material (nano-ePCM) dispersions as optical filters, heat carriers, and storage media in a double-pass PV/T system. Silica shells with paraffin-based PCM cores formed nano-ePCM. The system's performance was assessed by studying how the PCM's phase change affected PV cell operating temperatures and dispersions' spectral match values under different situations. PCM cores lowered PV cell operating temperatures during phase shift compared to non-phase change. In the liquid state, nano-ePCM dispersions (ePCM18, 26, and 32) had high spectral match values of 74.8%, 73.8%, and 70.9%, respectively, indicating efficient solar radiation filtering to align with silicon PV cell bandgaps. The prediction model predicts outcomes well against input variables it has not trained on. Heat transfer analysis increasingly uses artificial intelligence methods like the Artificial Neural Network (ANN) approach, which predicts thermal performance well.

Li, et al. [11] looked at how well a PV/T unit with an A2O3/water nanofluid-filled curved serpentine absorber tube worked regarding heat, electricity, and total efficiency. The system's performance measures are examined to see how Reynolds number (Re) and nanoparticle concentration (ω) affect them. The results show that the temperature of the PV panel drops by about 3.13 to 3.32% when the ς number goes from 0 to 1% and Re goes from 500 to 2000. On the other hand, this rise in Re causes a big drop in pressure, running from 5480.95 to 5580.06%. When ω goes from 0% to 1%, the temperature of the PV panel goes down by about 0.43 to 0.62% and the power needed for pumping goes down by about 1.25 to 2.97%. The total efficiency ranged from 60.38% to 90.45%, with Re = 2000 & ω = 1% having the highest value and Re = 500 & ω = 0% having the lowest value. The ANN modeling gave an exact function for figuring out how efficient the PVT unit under study was overall based on the factors Re and ω. The R-squared measure of prediction shows a high level of accuracy, $R^2 = 0.99602$.

After looking at previous research on cogeneration solar PV/T configurations, there is a need to figure out and investigate the various formations and evaluate thermal and electrical efficiency to improve the overall performance. This article focuses on PV/T collector integrating with the glazed cover in various configurations to assess the cogeneration system. Furthermore, this article theoretically examines all temperature fluctuations throughout the system. Ultimately, it evaluates thermal and electrical power, reporting the cogeneration performance and overall efficiency.

2. METHODS AND MATERIALS

A refined mathematical thermo-electrical model is established to assess the critical attributes of the cogeneration solar collector, employing advanced correlations to compute radiative heat losses and accounting for the influence of radiation heat transfer within the air duct. The methodology relies on a comparative analysis of four distinct configurations, as shown in Fig. 1. The four formations will be indicated throughout the paper as follows:

- PV-model (I): a basic photovoltaic panel that integrates the glazed cover.
- PV/T- Model (II): a cogeneration system that integrates the glazed cover.
- PV/T- Model (III): a cogeneration system that integrates the glazed cover and absorber plate.
- PV/T- Model (IV): a cogeneration system that integrates the glazed cover and absorber plate with a double pass.

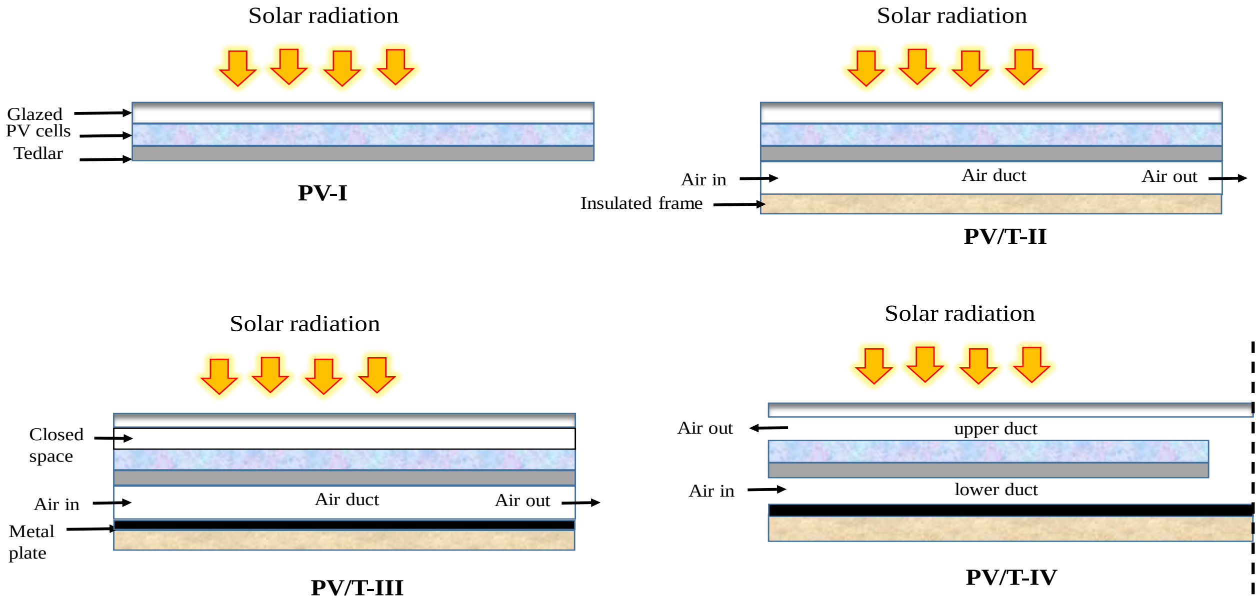

Fig. 1. The four formations of the tested cogeneration system.

2.1. SYSTEM DESCRIPTION

This study investigates cogeneration collector systems that utilize photovoltaic/thermal (PV/T) solar panels. It is established that approximately 15% of solar energy is reflected back into the environment upon incidence. In comparison, around 85% is absorbed by the photovoltaic cells. Under optimal conditions, these cells convert 10–25% of the absorbed solar energy into electrical energy, with the remainder being transformed into heat within the photovoltaic panel components. Elevated temperatures can accelerate the recombination of electron-hole pairs in the cells, leading to a reduction in the electrical output of the solar panel, thereby necessitating cooling measures. The proposed designs for the cogeneration collectors in configurations II, III, and IV are specifically engineered to cool the solar panels while simultaneously recovering the heat they lose. Notably, Model III features a glazed cover with an enclosed compartment above the PV panel to assess the impact of glazing on both thermal and electrical performance. Model IV incorporates an additional glazed lid and consists of two air channels: one situated beneath the PV panel and another below it. This design aims to optimize the heat exchange interface between the photovoltaic panel and the fluid, enhancing heat absorption efficiency. The dimensions of both the air duct and cogeneration collector are 1.28 m in length and 0.30 m in width, with a depth of 0.02 m calculated for both upper and lower ducts in a double-pass configuration.

2.2. SYSTEM ANALYSIS

It is important to keep in mind that the amount of electric power E_{el} that is generated by the photovoltaic panel of the PV/T is listed Rachid, et al. [12]:

$$E_{el} = I_{sun} A\, \eta_{cel} = I_{sun} A\, \eta_{ref} \left[1 - \beta_p (T_{cel} - T_{cell,ref})\right] \quad (1)$$

It is possible to write the equations that govern the dynamic energy balance for each layer, which are the glazed cover, the PV cell layer, and the insulator. [12, 13].

$$m_{gla} C_{gla} \frac{dT_{gla}}{dt} = A\left[\alpha_{gla} I_{sun} + h^{rd}_{gla}(T_{sky} - T_{gla}) + h^{cv}_{\frac{amb}{gla}}(T_{amb} - T_{gla}) - h^{cv}_{\frac{gla}{air}}(T_{gla} - T_{air}) + h^{rd}_{gla}(T_{gla} - T_{cell})\right] \quad (2)$$

$$m_{cell} C_{cell} \frac{dT_{cell}}{dt} = A\left[\tau_{gla}\alpha_{cell} I_{sun}\beta + h^{rd}_{\frac{gla}{cell}}(T_{gla} - T_{cell}) + h^{cv}_{\frac{cell}{air}}(T_{air} - T_{cell}) - h^{cv}_{\frac{cell}{ins}}(T_{ins} - T_{cell})\right] - E_{el}$$

$$m_{ins} C_{ins} \frac{dT_{ins}}{dt} = A\left[h^{cd}_{\frac{cell}{ins}}(T_{cell} - T_{ins}) + h^{cv}_{\frac{ins}{amb}}(T_{amb} - T_{ins})\right] \quad (3)$$

For the air channel, the equation that describes the balance of energy can be thought of as follows:

$$\dot{m}_{air} C_{air}(T_{out} - T_{in}) = A\left[h^{cv}_{\frac{glass}{air}}(T_{gla} - T_{air}) + h^{cv}_{\frac{cell}{air}}(T_{cell} - T_{air})\right] \quad (4)$$

Where,

$$T_{air} = \frac{T_{out} + T_{in}}{2} \quad (5)$$

In order to elucidate the balancing equations for all layers, several heat transfer models such as radiative, conductive, and convective methods, will be employed. The following subsections describe them analytically.

In the case of glazing and sky, the radiative heat transfer coefficient is as follows:

$$h^{\mathrm{rd}}_{\mathrm{gla}-sky} = \frac{\sigma\varepsilon_{glass}\left(T^4_{glass}-T^4_{sky}\right)}{T_{glass}-T_{amb}} \quad (6)$$

Where, $T_{sky} = 0.05\ T^{1.5}_{amb}$ (7)

The following equation can be used to calculate the heat transfer coefficient brought about by radiation between two infinite parallel plates (i, j):

$$h^{rd}_{i-j} = \frac{\sigma(T_i+T_j)\left(T_i^2+T_j^2\right)}{\frac{1}{\varepsilon_i}+\frac{1}{\varepsilon_j}-1} \quad (8)$$

The following equation can be used to calculate the conductive heat transfer coefficient between two layers (i, j):

$$h^{cd}_{i,j} = \left[\frac{l_i}{k_i}+\frac{l_j}{k_j}\right]^{-1} \quad (9)$$

In an air-based type, the convective heat transfer coefficients between air–Tedlar and air–the following relation can calculate the insulator:

$$h^{cv}_{air} = Nu\frac{k}{d} \quad (10)$$

Where k is air thermal conductivity, Nu is Nusselt number, and l is glazed tube length.

Heat transfer by convection of fluid flow inside an annular pipe where Reynold number Re and Prandtl number Pr are calculated as follows:

$$Re = \frac{\rho VD}{\mu} \quad (11)$$

$$Pr = \frac{\mu C_p}{k} \quad (12)$$

For laminar and turbulent flow, the Nusselt number can be estimated using Kays and Leung tables [14]. Otherwise, some works calculate it using the Dittus-Boelter model, as demonstrated in the article [15].

$$Nu = 0.023Re^{0.8}Pr^{n} \quad (13)$$

Where n = 0.4 for heating and 0.3 for cooling.

The total electrical and thermal efficiency of the PV/T collector can be expressed by Dimri, et al. [16]:

$$\eta_{th} = \frac{\dot{m}_f C_f(T_{fo}-T_{fi})}{I_t A_m} \quad (14)$$

The overall efficiency of the PV/T is obtained from this expression [17].

$$\eta_{\mathrm{overall}} = \eta_{\mathrm{th}} + \frac{\eta_t}{0.38} \quad (15)$$

Table 1 displays the used data, properties, and dimensions of all layers.

Table 1. Layer characteristics in the tested configurations.

Parameter	Value
Glazed	
Absorptivity (α_{gla})	0.06
Transmissivity (τ_{gla})	0.93
the emissivity (ε_{gla})	0.88
Thickness (L_{gla})	0.004 m
Thermal conductivity (k_{gla})	1.1 W/(m K)
Specific heat (C_{gla})	670 J/(kg K)
PV cell	
The emissivity (εcel)	0.96
Thickness (L_{cel})	0.0002 m
Absorptivity (α_{cel})	0.84
Specific heat (C_{cel})	900 J/(kg K)
Thermal conductivity (k_{cel})	140 W/(m K)
Tedlar	
The thickness (Lt)	0.00051 m
The thermal conductivity (kt)	0.032 W/m K
The absorptivity (αt)	0.81
Insulation	
Specific heat of insulation (C_{ins})	670 J/(kg K)
Thermal conductivity of insulation (k_{ins})	0.034 W/(m K)
Packing factor (β)	0.8
Temperature coefficient (β_P)	0.0045

2.3. VALIDATION

In the course of Joshi, et al. [18] investigation, the computer simulation model was compared to the work that Joshi and his colleagues had done. There was a comparison made between the findings of this study and those of Joshi et al. The PV panel is a conventional combination PV/T that makes use of a monocrystalline photovoltaic cell manufactured by Siemens as its source of energy. At the typical rating settings, this photovoltaic panel is capable of producing 75 watts of power. Within the context of this validation setting, the simulation model that is presented evaluates and evaluates how efficiently the system consumes energy. It uses the weather conditions from the experiment shown in Fig 2. Between the hours of 12:00 and 14:00, the solar radiation intensity reaches high values, in excess of 1000 W/m², on days when the sun is shining. The temperature of the surrounding air is between 30 and 40 degrees Celsius.

Experimental tests conducted using the given parameters and operating circumstances verify the validity of the analytical model. The outcomes show that the theoretical models and experimental findings are adhered to. The theoretical and experimental results differ by a respectable margin on average. The relative inaccuracy can be calculated as follows for a collection of data, such as the experimental power gained by solar air heaters and the numerical values given:

Firstly, the absolute error (AE) should be calculated as the absolute difference between the experimental value (Exp) and the simulation value (Sim) for each data point.

$$AE = |Exp - Num| \tag{16}$$

Secondly, compute the Relative Error (RE) as the ratio of the Absolute Error to the experimental value.

$$RE = \left(\frac{|Exp - Num|}{Exp}\right) \times 100\% \tag{17}$$

Fig. 3 shows the imagined temperatures of the cells and the air coming out of them, along with the actual temperatures measured on the test day. The experimental and generated graphics look a lot alike in this graph. The relative error for the exit air temperature is 3.98%, and the root mean square percent error is 4.52%. For the PV cells temperature, they are 3.40% and 3.65% each.

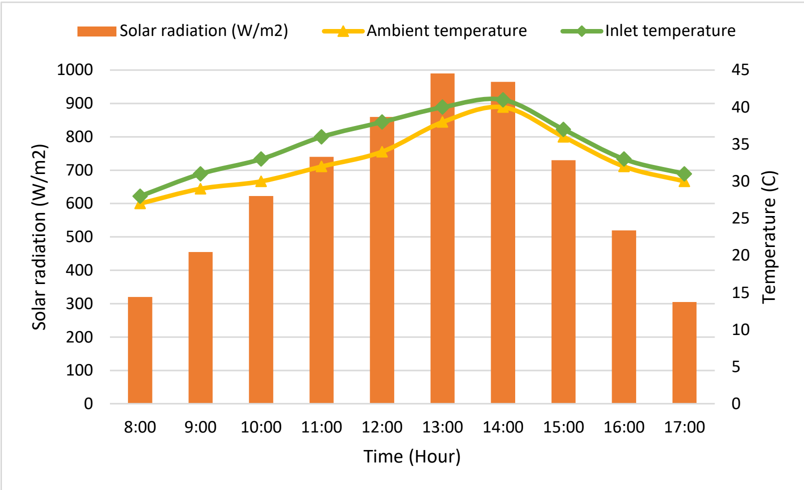

Fig. 2. The operation conditions during the tested time.

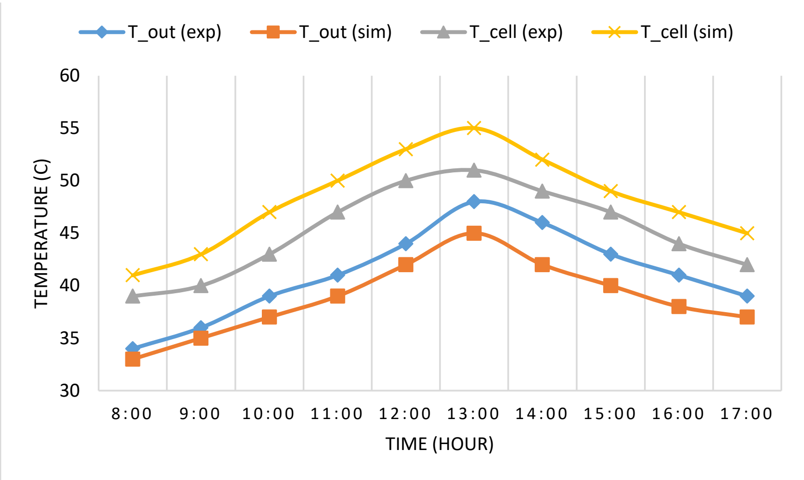

Fig. 3. Validation of outlet and cell temperature.

3. RESULTS AND DISCUSSIONS

The analysis of the cogeneration collector systems utilizing photovoltaic/thermal (PV/T) solar panels reveals significant insights into their thermal and electrical performance across the different configurations. This section will discuss the valuable aspects of results include temperature fluctuations, cogeneration performance, and overall efficiency.

3.1. TEMPERATURE FLUCTUATIONS

Error! Reference source not found. illustrates t he progression of different layers temperatures throughout each arrangement. The temperatures of PV/T layers are referred in the results curve as follows:

- **T_amb:** Ambient temperature
- **T_ted:** Temperature of the tedlar
- **T_abs:** Temperature of the absorber plate
- **T_cell:** Temperature of the solar cell
- **T_glass:** Temperature of the glass cover
- **T_out:** Temperature of the outlet air

The solar cells demonstrate the greatest temperatures among all configurations, recording values of 53, 48, 58, and 48 °C for (I, II, III, and IV) PV/T models, respectively. The glazed cover over the PV panel leads to a rise in temperature throughout all PV/T layers in Model (III). A dual fluid circulation system is necessary above the PV panel (IV) to alleviate these increased temperatures. The air temperature will rise, causing the augmented heat exchange surface between the air and the PV panel. The outlet temperature reaches a minimum of 27 °C at 08:00 throughout all PV/T models, attaining maximum values at 13:00 of 43°C, 44°C, and 48°C for models II, III, and IV, respectively. All temperatures of the PV/T components surpass the ambient temperature.

3.2. THERMAL AND ELECTRICAL POWER

Fig. 5 shows how each solar device's electricity per unit area changes every hour. At 8:00, all models produce relatively low power outputs, with Model II leading at 12 W/m². As the morning progresses, power output increases significantly. By 10:00, Model II reaches 55 W/m², while other models closely follow, indicating effective energy capture as solar radiation increases.

The maximum power output occurs around 13:00, where Model II achieves 106 W/m², followed closely by Model IV at 105 W/m². This peak reflects optimal conditions for solar energy conversion. The outputs for all models during this period indicate their ability to harness solar energy effectively, with all models exceeding 80 W/m². This peak reflects optimal conditions for solar energy conversion, characterized by maximum solar irradiance and favorable ambient temperatures that enhance the efficiency of photovoltaic cells. During this time, all models exceed 80 W/m², demonstrating their effectiveness in harnessing solar energy under ideal conditions.After reaching peak values, there is a noticeable decline in power output as the sun begins to set. By 15:00, Model II drops to 81 W/m², while Model IV decreases to 77 W/m². The decline continues into the evening hours, with outputs dropping significantly by 18:00 and further decreasing to around 6-7 W/m² by 19:00.

Model II consistently demonstrates the highest power output throughout the day, peaking at 106 W/m². This suggests that it has superior efficiency in converting solar energy into electrical power. Model IV follows closely behind, with a peak output of 105 W/m², indicating its effectiveness in energy conversion as well. Model I and Model III show lower outputs compared to Models II and IV, with maximum outputs of 104 W/m² and 102 W/m², respectively. This indicates that while they are functional, they may not be optimized for maximum energy capture and conversion. Notably, The rise in power output correlates with the increase in solar irradiance, which enhances the energy available for conversion into electricity. This period showcases how well-designed solar models can optimize their performance by adjusting to changing environmental conditions.

Fig. 6 illustrates the fluctuations of thermal power per unit area for each model of the cogeneration PV/T during the day. Notable value as the morning progresses, there is a significant increase in thermal power output. By 9:00, Model IV reaches 255 W/m², indicating effective heat absorption as solar radiation increases. The trend continues, with all models showing substantial gains in thermal power, peaking at 12:00. At this time, Model IV achieves its highest output of 560 W/m². The peak thermal power output occurs around 13:00, where Model IV reaches 590 W/m². This reflects optimal conditions for solar energy capture and conversion. Model III also performs well, achieving 488 W/m², while Model II reaches 373 W/m² during this hour. After reaching peak values, all models experience a decline in thermal power output as the sun begins to set. By 15:00, Model IV drops to 463 W/m². The decline continues into the evening hours, with outputs dropping significantly by 18:00 and further decreasing to around 10 W/m² by 19:00. Model IV consistently demonstrates the highest thermal power output throughout the day, particularly during peak solar hours. Its maximum output of 590 W/m² indicates its effectiveness in harnessing solar energy. Model III also shows strong performance, with a peak output of 488 W/m², suggesting it is well-designed for thermal energy capture. Model II exhibits lower thermal outputs compared to Models III and IV, with a maximum of only 373 W/m² during peak hours. This indicates potential limitations in its design or efficiency in heat transfer.

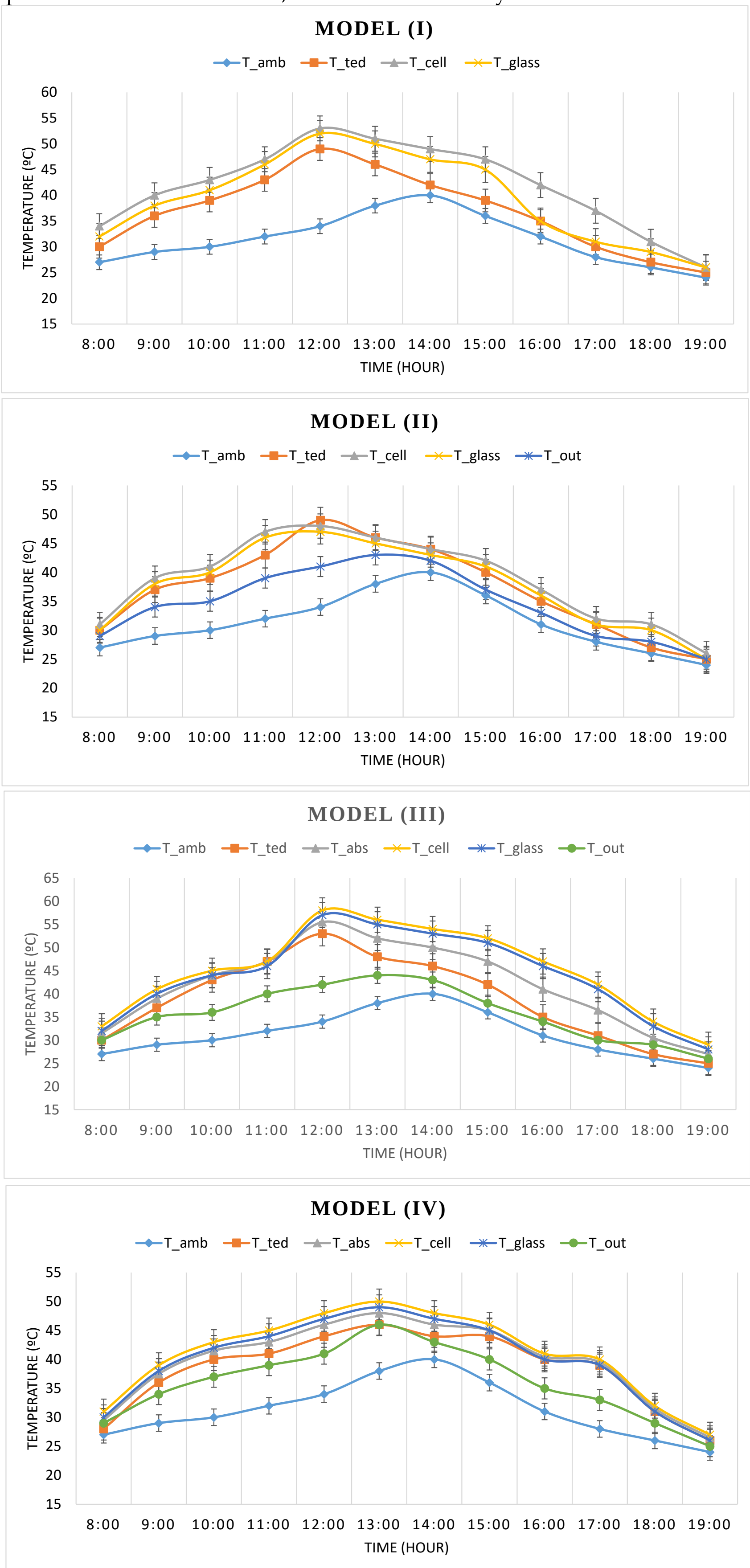

Fig. 4. Temperature fluctuations for the tested models.

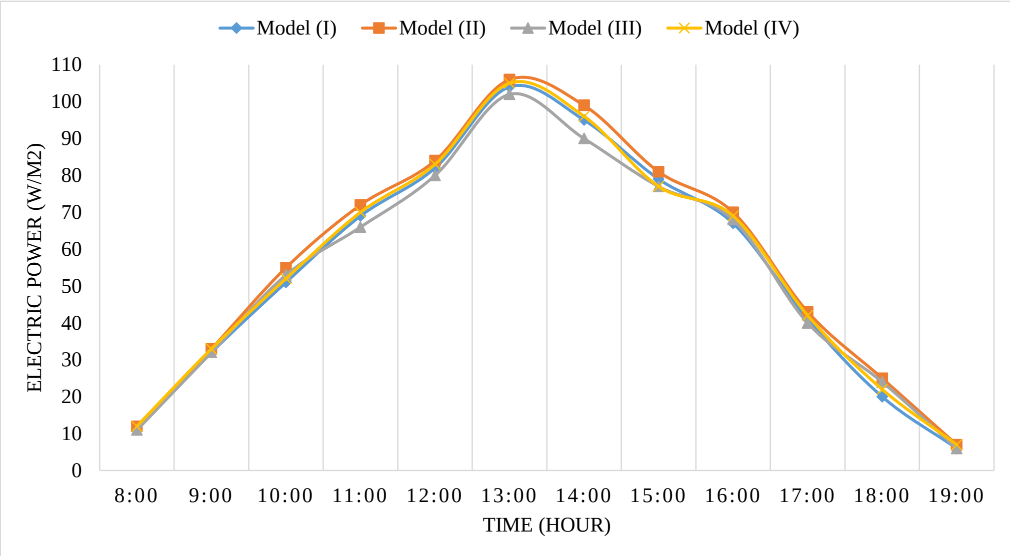

Fig. 5. Electrical power for the tested configurations.

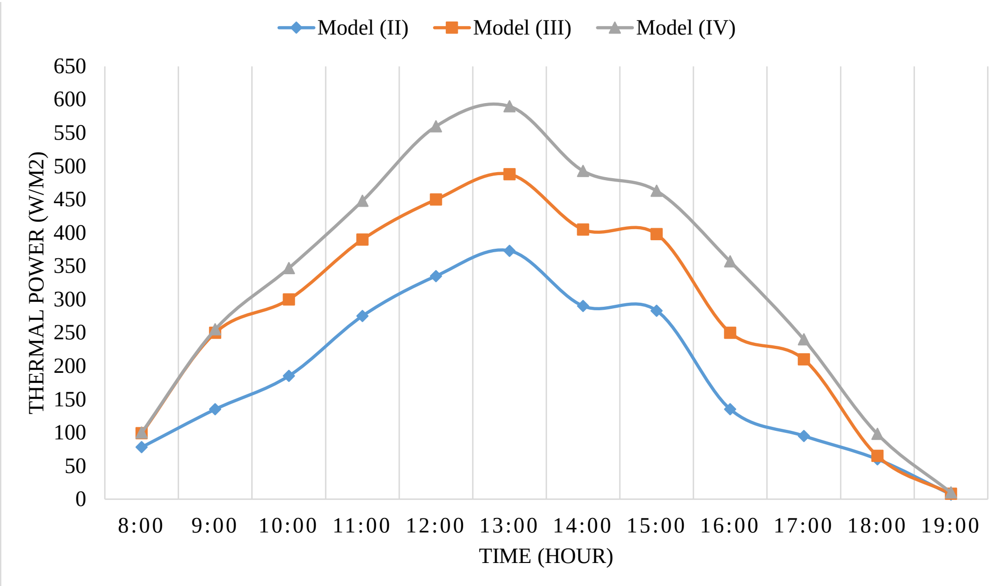

Fig. 6. Thermal power for different PV/T configurations.

3.3. THERMAL AND ELECTRICAL EFFICIENCY

An increase in the temperature of photovoltaic cells leads to a decrease in electrical efficiency. Fig. 7 depicts the comparative hourly variations in the electricity efficiency of each solar device.

At 8:00, all models exhibit similar electrical efficiencies, with Model II slightly ahead at 10.8%. As the morning progresses, efficiencies increase gradually for all models, peaking at 11.3% for Model II and Model IV by 9:00 and 10:00, respectively. During midday, electrical efficiencies tend to stabilize or decrease slightly across all models. Model IV maintains a consistent performance, achieving 11% at 11:00 and 12:00 PM, indicating robust efficiency under peak solar conditions. After reaching midday levels, there is a noticeable decline in electrical efficiency as the day progresses. By 19:00, model I drops to 10.5%, while Model IV ends the day at 10.4%. Model II consistently shows the highest electrical efficiency during the morning and early afternoon hours, peaking at 11.3% at both 9:00 and 17:00. Model IV performs competitively with a peak efficiency of 11%, indicating its effectiveness in maintaining performance throughout varying conditions. Model III generally lags behind the others, with its maximum efficiency reaching only 11%, suggesting potential design limitations or less effective energy conversion capabilities.

Fig. 8 depicts the comparative hourly variations in thermal efficiency for three models of the cogeneration PV/T collector. Model IV shows a strong start with an efficiency of 30% at 8:00, rising to a peak of 63% by 11:00. This indicates effective heat absorption and conversion during the early hours. Model III also performs well, starting at 29% and reaching 50% by 11:00. In contrast, Model II begins with a lower efficiency of 10%, peaking at only 32% by 13:00, indicating less effective thermal performance compared to the other models. During peak solar radiation at noon, Model IV maintains high efficiency at 62%, slightly lower than its peak but still superior to the other models. Model III remains competitive with an efficiency of 51%, while Model II struggles to keep pace, showing only 31%. After noon, all models experience a decline in thermal efficiency as solar radiation decreases. Model IV remains the most efficient throughout the afternoon, fluctuating between 59% and 61% until late afternoon. Model III shows a gradual decline but maintains better performance than Model II, which drops sharply to only 9% by evening. Model IV consistently outperforms the other two models across all time intervals, indicating superior design or materials that enhance thermal absorption and retention capabilities. The uniform cooling of the solar panel using double flow lowers the temperature of the photovoltaic cells, hence improving the panel's electrical conversion efficiency. The absorber plate situated above the thermal insulator improves heat transfer through radiation with the solar panel, hence lowering the panel's temperature. Model III demonstrates relatively stable performance but does not reach the efficiency levels of Model IV during peak times. Its ability to maintain higher efficiencies than Model II suggests it is a viable option but may require improvements for optimal performance. Model II's lower efficiencies throughout the day highlight potential design limitations or inefficiencies in heat transfer mechanisms. Its performance is significantly behind that of Models III and IV, particularly during peak sunlight hours.

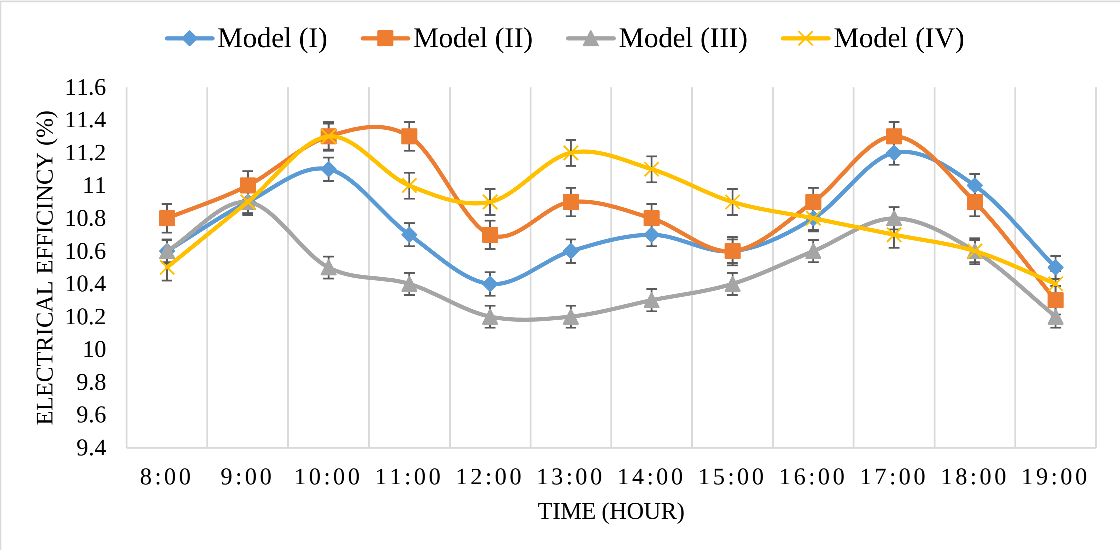

Fig. 7. Electrical efficiency for the tested configurations.

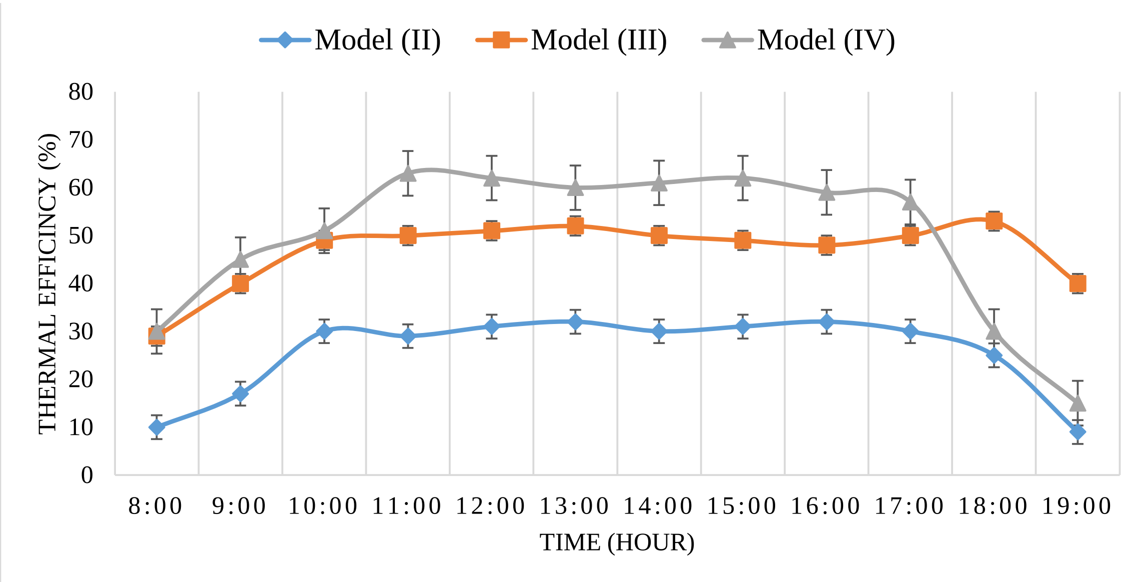

Fig. 8. Thermal efficiency for different PV/T configurations.

3.4. OVERALL ENERGY EFFICIENCY

Fig. 9 depicts the hourly variations in overall energy efficiency of each solar device. Model IV starts with an efficiency of 32% at 8:00 and shows a notable increase throughout the morning, reaching 90% by 11:00. Model III also demonstrates strong performance, starting at 45% and peaking at 70% by 11:00. model I and Model II have relatively lower efficiencies, with Model II peaking at 60% by 11:00. At noon 12:00, Model IV achieves its highest efficiency at 92%, indicating optimal performance under peak solar radiation. Model III follows closely with an efficiency of 77%, while Models I and II lag behind, showing efficiencies of 29% and 61%, respectively. After reaching peak values, all models begin to experience a decline in efficiency as the sun starts to set.

Model IV remains the most efficient throughout the afternoon, maintaining above 80% until 17:00, then dropping to 42% by 19:00. Model III shows a gradual decrease from a high of 85% at 5:00 to 76% by 19:00, while Models I and II experience sharper declines.

Model IV consistently outperforms the other models throughout the day, particularly during peak sunlight hours. Its design appears to effectively harness solar energy while maintaining high efficiency. Model III also exhibits commendable performance but falls short compared to Model IV, especially in the late morning and early afternoon when solar radiation is at its peak. Models I and II show lower overall efficiencies throughout the day. Model II peaks at only 61% during midday, indicating potential limitations in heat collection or conversion capabilities compared to Models III and IV.

As solar radiation increases during the morning and peaks around noon, models that are better designed for heat absorption (like Model IV) show higher efficiencies. Higher ambient temperatures can affect the thermal performance of collectors; however, Model IV manages to maintain efficiency even as temperatures begin to drop in the afternoon. The decline in efficiency post-peak hours is expected due to reduced solar radiation availability. However, the rate of decline varies significantly among models, with Models I and II experiencing steeper drops.

3.5. COMPARISON WITH RELEVANT STUDIES

The performance of PV/T air collectors is a critical area of research, particularly in optimizing their thermal and electrical efficiencies for enhanced energy output. Thermal efficiency (ηth) in PV/T air collectors can vary widely, depending on factors such as air mass flow rates and design configurations. For instance, a significant increase in thermal efficiency has been observed with higher air mass flow rates, attributed to improved heat transfer between the photovoltaic module and the flowing air. Electrical efficiency (ηele) typically ranges from 9% to 22%, influenced by the cooling effects of the air passing through the collector. This helps maintain optimal operating temperatures for the photovoltaic cells. Overall efficiency (η overall), which combines both thermal and electrical efficiencies, makes these systems particularly advantageous in applications where space is limited. The integration of advanced designs, such as dual-pass configurations and the use of fins or baffles, has been shown to further enhance both thermal and electrical performance. Table 2 provides a comparison with different PV/T configurations and indicates the thermal and electrical efficiencies.

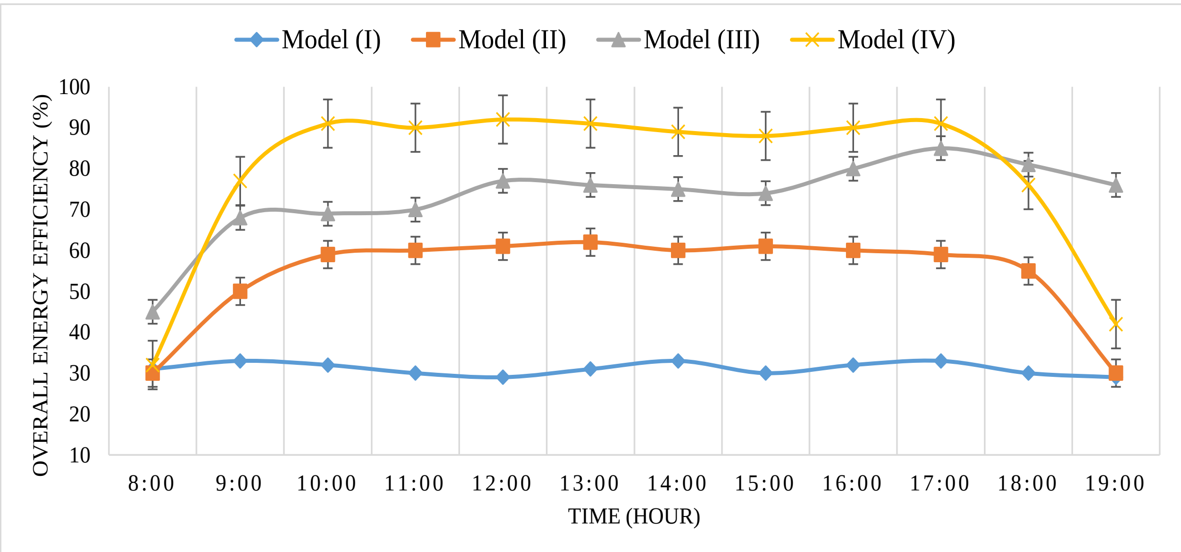

Fig. 9. Overall energy efficiency for the tested configurations.

Table 2. Comparison with relevant studies that were earlier published.

Author	Description	η th	η el	η overall
Chen, et al. [19]	It presents a configuration of a PV/T air collector with a closed structure and a glass cover. An experimental stage for collector performance testing was constructed, aiming to investigate the thermal and electrical performance under laboratory conditions.	49.3 %	10.4 %	71.1
Dunne, et al. [20]	The performance of a PV/T air collector is evaluated by revealing the temperature distribution and investigating the effect of the inlet and outlet air temperature and PV cell temperature.	13.57	36.45 %	74.14 %
Diwania, et al. [21]	Assess the performance of the PV/T air collector on the basis of the data obtained from the cloud server	42.6 %	12.6 %	-
Nazri, et al. [22]	Proposed hybrid system enhances the conversion efficiency of PV cells by incorporating an intelligent thermal management system, which leverages the dual functions of thermoelectric	14.04%	57 %	-
Dunne, et al. [23]	Investigates the performance of a novel air-type PV/T combined with a transverse triangle obstacle under various geometric condition.	17.01%	39.04%	-
Khelifa, et al. [24]	The efficient multiple-impinging slot jets were incorporated with the bottom surface of the cooling channels to enhance the overall efficiency of PVT collectors and optimize the design of the developed cooling.	22.26%	35.07%	91.42 %
Present study	Focuses on PV/T collector integration with the glazed cover in various configurations to assess the cogeneration system. A glazing double-pass PV/T cogeneration system with an absorber layer was a standard model.	11.2%	61.23%	92.36%

4. Conclusions

This study conducted a comparative analysis of the thermal and electrical efficiencies of four models of photovoltaic/thermal air collectors (Model I, Model II, Model III, and Model IV) across various time intervals throughout the day. The data collected highlights significant differences in performance among the models, providing insights into their operational efficiencies under varying environmental conditions.

- Model IV consistently outperformed the other models in thermal efficiency throughout the day, achieving peak values of **92%** during midday. This superior performance can be attributed to its effective design and materials that enhance heat absorption and retention capabilities.
- Model III demonstrated commendable thermal efficiency but did not reach the levels of Model IV. In contrast, Model II exhibited significantly lower thermal efficiencies, particularly during peak solar hours, indicating potential limitations in its design or heat transfer mechanisms.
- In terms of electrical efficiency, Model II emerged as the most efficient model overall, with a peak efficiency of 11.3% during the morning and early afternoon hours. This suggests that it effectively converts solar energy into electrical power under optimal conditions.
- Model IV maintained competitive electrical efficiency levels, peaking at 11%, while Model III lagged behind with maximum efficiencies of around 11%. The consistent performance of models II and IV highlights their effectiveness in energy conversion.
- All models exhibited a general trend of increased efficiency during the morning hours, peaking around midday before experiencing a decline in the afternoon as solar radiation diminished. The ability to maintain higher efficiencies in the afternoon varied significantly among models, with Model IV demonstrating better retention compared to Models I and II.

References

[1] A. Elbrashy, Y. Boutera, M. M. Abdel-Aziz, S. Dafea, and M. Arıcı, "A review on air heating applications with evacuated tubes: A focus on series and parallel tube configurations," *Solar Energy*, vol. 264, p. 111996, 2023/11/01/ 2023, doi: https://doi.org/10.1016/j.solener.2023.111996.

[2] M. A. Elazab *et al.*, "Exergoeconomic assessment of a multi-section solar distiller coupled with solar air heater: Optimization and economic viability," *Desalination and Water Treatment,* vol. 319, p. 100535, 2024/07/01/ 2024, doi: https://doi.org/10.1016/j.dwt.2024.100535.

[3] M. Reda, M. E. Ali, S. Sharshir, and I. El-Kalla, "Novel fractional modeling based on CATTANEO heat flux for enhancing thermal performance of u-tube parabolic trough collectors," *Journal of Contemporary Technology and Applied Engineering,* vol. 3, no. 1, pp. 75-87, 2024, doi: 10.21608/jctae.2024.302870.1031.

[4] A. Alkhalidi, T. Salameh, and A. Al Makky, "Experimental investigation thermal and exergy efficiency of photovoltaic/thermal system," *Renewable Energy,* vol. 222, 2024, doi: 10.1016/j.renene.2023.119897.

[5] A. P. Singh, S. Tiwari, and H. Sinhmar, "Modelling and analysis of photovoltaic-thermal-thermoelectric-cooler air collector integrated mixed-mode greenhouse dryer with heat storage material," *Journal of Energy Storage,* vol. 95, p. 112369, 2024/08/01/ 2024, doi: https://doi.org/10.1016/j.est.2024.112369.

[6] I. Lamaamar, A. Tilioua, and M. A. Hamdi Alaoui, "Thermal performance analysis of a poly c-Si PV module under semi-arid conditions," *Materials Science for Energy Technologies,* vol. 5, pp. 243-251, 2022, doi: 10.1016/j.mset.2022.03.001.

[7] M. R. Sharaby, M. Younes, F. Baz, and F. Abou-Taleb, "State-of-the-Art Review: Nanofluids for Photovoltaic Thermal Systems," *Journal of Contemporary Technology and Applied Engineering,* vol. 3, no. 1, pp. 11-24, 2024, doi: 10.21608/jctae.2024.288445.1025.

[8] B. Limane, C. Ould-Lahoucine, and S. Diaf, "Modeling and simulation of the thermal behavior and electrical performance of PV modules under different environment and operating conditions," *Renewable Energy,* vol. 219, 2023, doi: 10.1016/j.renene.2023.119420.

[9] M. Herrando, G. Fantoni, A. Cubero, R. Simón-Allué, I. Guedea, and N. Fueyo, "Numerical analysis of the fluid flow and heat transfer of a hybrid PV-thermal collector and performance assessment," *Renewable Energy,* vol. 209, pp. 122-132, 2023, doi: 10.1016/j.renene.2023.03.125.

[10] A. T. Hamada, O. Z. Sharaf, and M. F. Orhan, "A novel photovoltaic/thermal (PV/T) solar collector based on a multi-functional nano-encapsulated phase-change material (nano-ePCM) dispersion," *Energy Conversion and Management,* vol. 280, 2023, doi: 10.1016/j.enconman.2023.116797.

[11] L. Li *et al.*, "Prediction of heat transfer characteristics and energy efficiency of a PVT solar collector with corrugated-tube absorber using artificial neural network and group method data handling models," *International Communications in Heat and Mass Transfer,* vol. 157, 2024, doi: 10.1016/j.icheatmasstransfer.2024.107829.

[12] A. Rachid, A. Goren, V. Becerra, J. Radulovic, and S. Khanna, "Solar PVT Systems," in *Solar Energy Engineering and Applications*, A. Rachid, A. Goren, V. Becerra, J. Radulovic, and S. Khanna Eds. Cham: Springer International Publishing, 2023, pp. 83-104.

[13] A.-G. Lupu, E. Hristoforou, G.-D. Tcaciuc, and A. Popescu, "Theoretical Model for Photovoltaic Panel Thermal Analysis," *Bulletin of the Polytechnic Institute of Iași. Machine constructions Section,* vol. 68, no. 1, pp. 79-88, 2022, doi: 10.2478/bipcm-2022-0006.

[14] W. M. Kays and E. Y. Leung, "Heat transfer in annular passages—hydrodynamically developed turbulent flow with arbitrarily prescribed heat flux," *International Journal of Heat and Mass Transfer,* vol. 6, no. 7, pp. 537-557, 1963/07/01/ 1963, doi: https://doi.org/10.1016/0017-9310(63)90012-7.

[15] J. Dirker and J. P. Meyer, "Convective Heat Transfer Coefficients in Concentric Annuli," *Heat Transfer Engineering,* vol. 26, no. 2, pp. 38-44, 2005, doi: 10.1080/01457630590897097.

[16] N. Dimri, A. Tiwari, and G. N. Tiwari, "Effect of thermoelectric cooler (TEC) integrated at the base of opaque photovoltaic (PV) module to enhance an overall electrical efficiency," *Solar Energy,* vol. 166, pp. 159-170, 2018/05/15/ 2018, doi: https://doi.org/10.1016/j.solener.2018.03.030.

[17] S. Tiwari and G. N. Tiwari, "Energy and exergy analysis of a mixed-mode greenhouse-type solar dryer, integrated with partially covered N-PVT air collector," *Energy,* vol. 128, pp. 183-195, 2017/06/01/ 2017, doi: https://doi.org/10.1016/j.energy.2017.04.022.

[18] A. S. Joshi, A. Tiwari, G. N. Tiwari, I. Dincer, and B. V. Reddy, "Performance evaluation of a hybrid photovoltaic thermal (PV/T) (glass-to-glass) system," *International Journal of Thermal Sciences,* vol. 48, no. 1, pp. 154-164, 2009, doi: 10.1016/j.ijthermalsci.2008.05.001.

[19] Y. Chen *et al.*, "A comparative experimental study on the performance of photovoltaic thermal air collectors," *Applied Thermal Engineering,* vol. 248, 2024, doi: 10.1016/j.applthermaleng.2024.123109.

[20] N. A. Dunne, P. Liu, A. F. A. Elbarghthi, Y. Yang, V. Dvorak, and C. Wen, "Performance evaluation of a solar photovoltaic-thermal (PV/T) air

collector system," *Energy Conversion and Management: X,* vol. 20, p. 100466, 2023/10/01/ 2023, doi: https://doi.org/10.1016/j.ecmx.2023.100466.

[21] S. Diwania, M. Kumar, V. Gupta, S. Agrawal, P. Khetrapal, and N. Gupta, "Insight into the Investigation of Thermo-Electrical Performance of Hybrid Photovoltaic-Thermal Air-Collector," *Journal of The Institution of Engineers (India): Series B,* vol. 105, no. 5, pp. 1275-1283, 2024, doi: 10.1007/s40031-024-01040-z.

[22] N. S. Nazri *et al.*, "Analytical and experimental study of hybrid photovoltaic–thermal–thermoelectric systems in sustainable energy generation," *Case Studies in Thermal Engineering,* vol. 51, 2023, doi: https://doi.org/10.1016/j.csite.2023.103522.

[23] N. A. Dunne, P. Liu, A. F. A. Elbarghthi, Y. Yang, V. Dvorak, and C. Wen, "Performance evaluation of a solar photovoltaic-thermal (PV/T) air collector system," *Energy Conversion and Management: X,* vol. 20, 2023, doi: 10.1016/j.ecmx.2023.100466.

[24] A. Khelifa, M. Abdelgaied, K. Harby, and M. El Hadi Attia, "Performance improvement of photovoltaic/thermal collectors based on the optimized design of efficient innovative multiple-impinging slot jets," *Solar Energy,* vol. 283, p. 112992, 2024/11/15/ 2024, doi: https://doi.org/10.1016/j.solener.2024.112992.